



Universiteit
Leiden
The Netherlands

Technical advances in multi-slice computed tomography : dose assessment and clinical optimizations

Joemai, R.M.S.

Citation

Joemai, R. M. S. (2012, June 12). *Technical advances in multi-slice computed tomography : dose assessment and clinical optimizations*. Retrieved from <https://hdl.handle.net/1887/19075>

Version: Corrected Publisher's Version

License: [Licence agreement concerning inclusion of doctoral thesis in the Institutional Repository of the University of Leiden](#)

Downloaded from: <https://hdl.handle.net/1887/19075>

Note: To cite this publication please use the final published version (if applicable).

Cover Page



Universiteit Leiden



The handle <http://hdl.handle.net/1887/19075> holds various files of this Leiden University dissertation.

Author: Joemai, Raoul M. S.

Title: Technical advances in multi-slice computed tomography : dose assessment and clinical optimizations

Date: 2012-06-12

7

Development and validation of segmentation and interpolation techniques in sinograms for metal artifact suppression in CT

Veldkamp WJ, Joemai RM, van der Molen AJ, Geleijns J.
Med Phys. 2010 Feb;37(2):620-8.

Abstract

Objective. Metal prostheses cause artifacts in computed tomography (CT) images. The purpose of this work was to design an efficient and accurate metal segmentation in raw data to achieve artifact suppression and to improve CT image quality for patients with metal hip or shoulder prostheses.

Materials and methods. The artifact suppression technique incorporates two steps: metal object segmentation in raw data and replacement of the segmented region by new values using an interpolation scheme, followed by addition of the scaled metal signal intensity. Segmentation of metal is performed directly in sinograms, making it efficient and different from current methods that perform segmentation in reconstructed images in combination with Radon transformations. Metal signal segmentation is achieved by using a Markov random field model (MRF). Three interpolation methods are applied and investigated. To provide a proof of concept, CT data of five patients with metal implants were included in the study, as well as CT data of a PMMA phantom with Teflon, PVC, and titanium inserts. Accuracy was determined quantitatively by comparing mean Hounsfield (HU) values and standard deviation (SD) as a measure of distortion in phantom images with titanium (original and suppressed) and without titanium insert. Qualitative improvement was assessed by comparing uncorrected clinical images with artifact suppressed images.

Results. Artifacts in CT data of a phantom and five patients were automatically suppressed. The general visibility of structures clearly improved. In phantom images, the technique showed reduced SD close to the SD for the case where titanium was not inserted, indicating improved image quality. HU values in corrected images were different from expected values for all interpolation methods. Subtle differences between interpolation methods were found.

Conclusion. The new artifact suppression design is efficient, for instance, in terms of preserving spatial resolution, as it is applied directly to original raw data. It successfully reduced artifacts in CT images of five patients and in phantom images. Sophisticated interpolation methods are needed to obtain reliable HU values close to the prosthesis.

Introduction

Metal implants such as prosthetic devices, dental fillings, surgical clips, and electrodes produce streak artifacts on the computed tomography (CT) images. The artifacts arise during the process of filtered back projection (FBP), which is the common image reconstruction technique in CT, and they appear as dark and bright streaks and bands in the reconstructed volume. The causes are fourfold: (1) significant beam hardening due to the metal object in combination with the broad x-ray spectrum in most CT scanners, (2) poor signal-to-noise ratio from photon starvation in the metal region, (3) scatter, and (4) edge-gradient effects.^{1,2} The metal artifacts that arise seriously limit the clinical value of the CT scan since they affect diagnosis and radiotherapy treatment planning. The need for improved metal artifact reduction in computed tomography grows with the increasing importance of CT imaging. The development of optimal metal artifact reduction in CT is particularly relevant considering that 3D imaging with MRI is not effective for patients with certain types of metal prostheses.

In routine practice a slight reduction in metal artifacts can be achieved by selecting appropriate acquisition parameters such as high tube voltage and high tube current. Iterative reconstruction methods are less susceptible for metal artifacts but these reconstruction methods have other drawbacks such as long reconstruction times.³ Several image processing solutions have been provided to remove artifacts caused by metal implants. The first publications on metal artifact reduction were by Glover et al.⁴ in 1981 and by Kalender et al.⁵ in 1987. The image-based method by Kalender et al., for instance, comprised segmentation of the metal implant in reconstructed images. An advantage is that segmentation in reconstructed CT images is relatively easy since these images do not substantially suffer from overprojection. Moreover, pixel values do not vary substantially within materials, facilitating segmentation in these kinds of images. In addition to segmentation of the metal prosthesis, projection data of the metal object were created using a Radon transformation. Linear interpolation was performed in the projected metal region in original raw data to substitute the metal signal by lower intensities. A filtered backprojection finally used to create a new image with improved image quality. It should be noted that reprojecting regions to Radon space in the same geometry as the original raw data may be quite complicated, especially in the case of modern multirow detector spiral data.⁶ As an alternative, artificial raw data, created from reconstructed slices using a simpler geometry, can be used instead of original raw data.³ A disadvantage of this latter approach is that generation of artificial raw data from a reconstructed image as a base for the correction is suboptimal in terms of spatial resolution. The additional necessary forward projection and tomographic reconstruction steps in the postprocessing application have a low-pass filtering effect on the corrected images. This is visually perceivable as a lower image contrast.³

Most subsequent publications describe similar approaches of segmentation in reconstructed images, interpolation in raw data, and backprojection of the modified raw data.^{2, 5, 7-11} However, different interpolation techniques are used in these publications (e.g., linear, b-spline, cubic spline, and wavelet interpolation). A more sophisticated approach for substituting the metal signal by more appropriate intensities is described by Bal and Spies.³ They use clustering of materials in reconstructed images followed by forward projection to optimally substitute the metal region in artificially created raw data by clustered raw data.

Implementing segmentation and correction directly in original raw CT data or sinograms would avoid the need for a computationally complex forward projection with the same geometry as the original raw data (or the disadvantage associated with using artificial raw data). Moreover, such approach can correct for metal artifacts that originate from a prosthesis that is positioned (partly) outside the field of view. In such images, metal of course cannot be segmented in reconstructed images. We propose correction in original raw data, realized by segmentation of the projections of the metal objects directly in raw data followed by interpolation in the segmented areas. Subsequently, a scaled version of the estimated original metal signal is added to the interpolation result. This in order to replace the metal signal by a more appropriate signal intensity and to preserve a realistic representation of the shape of the prosthesis in the corrected reconstructed images. Sophisticated segmentation of the raw data is required since simple methods, such as thresholding techniques combined with morphologic operations, appeared not feasible in pilot studies.¹² To evaluate our raw data-based method, we performed phantom tests for quantitative analysis. We additionally performed clinical tests based on scans of five patients with hip or shoulder prostheses.

Materials and Methods

General overview of data handling

CT scans in this study were performed using a Toshiba Aquilion 64 MSCT scanner (Toshiba Medical Systems, Otawara, Japan). Logistically the procedure in this study was as follows: in cooperation with Toshiba Medical Systems, raw data could be transferred from the CT scanner to a dedicated personal computer. These raw data are in the form of a logarithm of the normalized transmission, i.e., the transmission (I) normalized to the unattenuated beam (I_0). Raw data were then processed in order to suppress the metal artifacts. Modified raw data were transferred back to the scanner and reconstructed at the scanner with routine clinical protocols.

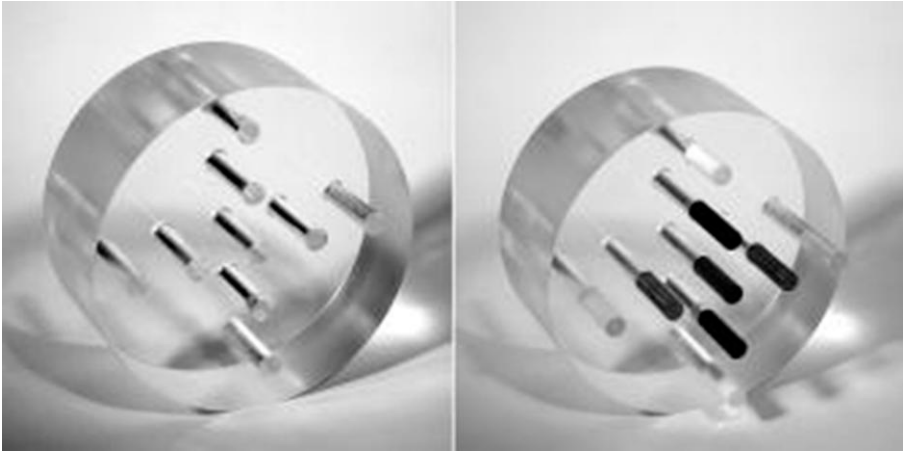


Figure 1 A PMMA phantom was constructed for investigating the impact of the artifact reduction methods. At the left, the phantom is shown without inserts. At the right, the phantom is shown together with some inserts.

Image acquisition

Phantom data

Figure 1 shows the polymethyl methacrylate (PMMA) phantom used in this study. The phantom has dimensions of 15 cm depth×32 cm diameter. The phantom contains nine holes with a diameter of 1.5 cm. The inserts were constructed from different materials: Teflon simulating bone, polyvinyl chloride (PVC) simulating fat tissue, and titanium simulating metal prostheses.

Two spiral acquisitions of the phantom were performed: one with titanium insert and one without titanium insert (a PMMA insert was used instead). Data acquisition concerning the phantom was performed using the following parameters: beam collimation of 64×0.5 mm, tube voltage of 120 kV, tube current of 350 mA, and scan field of view of 400 mm. All images were reconstructed at 1 mm slice thickness and 1 mm reconstruction interval. The images were reconstructed with a soft convolution kernel (FC12).

Patient data

Spiral CT scans of five patients with unilateral prosthesis were acquired: four patients have shoulder prostheses and one patient has a hip prosthesis. Data acquisition was performed using the following parameters: beam collimation of 64×0.5 mm, tube voltage of 120–135 kV, variable tube current (automatic exposure control was used), and scan field of view of 400–500 mm. All images were reconstructed at 1 mm slice thickness and 1 mm reconstruction interval. The images were reconstructed with a soft convolution kernel (FC12).

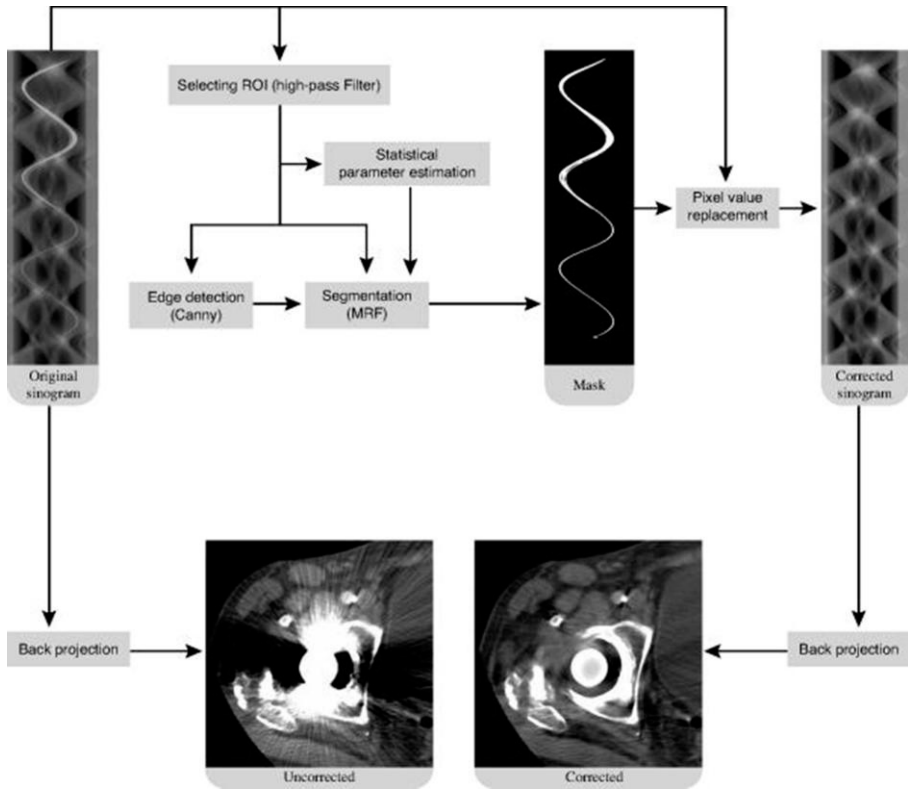


Figure 2 General overview of the method. It comprises high-pass filtering and thresholding, followed by automatic selection of a region of interest. Segmentation in the ROI is achieved by using raw sinogram data, pixel value statistics, and the output of an edge filter. Finally, replacement of pixel values in the metal region is achieved based on inward interpolation of the adjacent background and scaling of the original metal signal.

Metal artifact suppression

Suppression of metal artifacts by adapting raw data is based on two main steps: segmentation of the metal signal in the original sinogram and replacement of raw data pixels in the metal region by more appropriate values. An overview of the method in more detail is given in Fig. 2. It comprises high-pass filtering and thresholding, followed by automatic selection of a region of interest (ROI). Segmentation in the ROI is achieved by using raw data (sinogram), pixel value statistics, and the output of an edge filter. Finally, replacement of pixel values in the metal region is achieved based on interpolation from the adjacent background and scaling of the original metal signal intensity.

Segmentation of the metal implant

Software was developed in MATLAB (MatLab R2007a, The MathWorks Inc.,

Natick, MA). Segmentation was performed in the sinograms for each of the 64 detector rows. The columns in a sinogram correspond with the detector elements in the corresponding detector row. The number of rows in the sinograms is determined by the product of the number of views per rotation and the total number of rotations (each row corresponds with a projection angle). To perform a first segmentation, a copy of the raw CT data, reduced in size by a factor of 4 (i.e., 2 by 2 binning of the pixels), was used to reduce processing time, and then high-pass filtered followed by thresholding. High-pass filtering was done using a Gaussian high-pass filter ($\sigma = 5$). The threshold is determined automatically based on a method described earlier.¹³ First the object in the high-pass filtered image is roughly detected using a fixed threshold that was set at the 95 percentile of the pixel values. This threshold appeared to be robust with respect to both unilateral and bilateral prostheses. Note that a hip or shoulder prosthesis gives a substantial high filter output relative to other structures. This initial threshold is then used to collect statistics on the foreground and background regions obtained; the mean pixel value for all pixels below the threshold is determined (T_b), and the mean level of pixels greater than or equal to the initial threshold is determined (T_o). A new estimate of the threshold is computed as an average of the mean levels in each pixel class [calculated as $(T_b+T_o)/2$], and the process is repeated using this threshold. When no change in threshold is found in two consecutive passes through the image, the process stops. In our experiments this was generally the case after five passes.

The mask obtained by thresholding is converted to original high resolution and used as a ROI containing the metal implant in the original high resolution data. Figures 3a,3b show, respectively, part of the mask and the corresponding original sinogram. Note from the figure that the metal prosthesis is represented by several traces in the sinogram. This is due to the fact that the prosthesis comprises different components as a head, a cup, and screws. A Markov random field model (MRF model) in combination with Bayesian techniques is applied to obtain the final optimized segmentation result. The MRF model is specified by the labeling of a pixel on the basis of the conditional probability distribution given its gray level and the labels of its neighbors. The method used here is based on earlier publications.¹⁴⁻¹⁶ With respect to the labeling we consider foreground (metal signal) and background as label. A Gaussian model is used for representing the fluctuation of the raw data values y . The resulting model is described by the following equation:

$$\log P(x_i = l | (y_i, \text{other labels})) \propto -\alpha(l) + \beta(l)g(l) + \gamma(l)h(C) - (y_i - \mu_l)^2 / (2\sigma_l^2), \quad (1)$$

where x_i is a label of pixel i which can take two values l (background: $l = 0$; and foreground: $l = 1$, respectively) and $\alpha(l)$ is an offset value. The interaction parameter β models the *a priori* likelihood of labels to occur close to each other where $g(l)$ is the number of neighbors with class l . The neighborhood that is used here consists of the 24 neighbors in a 5×5 pixel window centered at pixel site i . The product of interaction parameter $\gamma(l)$ and function $h(C)$ models the

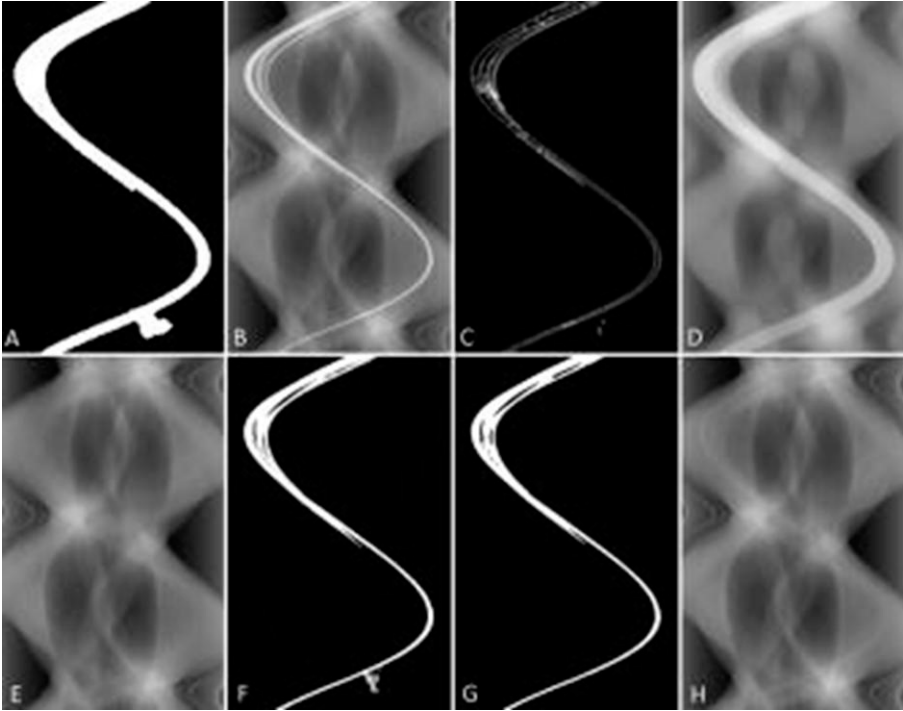


Figure 3 Patient with hip replacement. The MRF method is used to segment the metal implant at the original raw data. (a) shows the first segmentation after high-pass filtering and thresholding. (b) shows the ROI corresponding with (a). The Markov random field uses the original data (b), the output of a Canny filter (c), and estimates of the mean local metal signal (d) and background signal (e). A first result of the MRF method is shown in (f). After ten iterations the final segmentation result is obtained (g) and this result is used to correct raw data in the corresponding region (h).

interaction with edges in the MRF. Finally, y_i represents the pixel value of pixel x_i and the parameters μ_i and σ_i model the statistical distribution of pixel values.

A pixel is more likely to be part of the metal signal if it is located in the neighborhood of edges (represented by strong gradients). Modeling interaction with edges is especially helpful in parts where the implant becomes thinner and the difference in pixel intensity between foreground and background is reduced. A Canny filter (MATLAB built-in function; low and high thresholds, respectively: 0.1 and 0.2; $\sigma = 1.0$) is applied in the ROI for obtaining a representation of the edges of the implant. The function $h(C)$ is defined on the current edge pattern C . To be precise, C represents the edge pattern (Canny filter output) within the current estimate of the foreground. The function $h(C)$ defines for each pixel site i a specific value. These values are derived by applying a Gaussian low-pass filter ($\sigma = 3$; kernel size: 18×18 pixels) to C to model interaction with edges on a wider range [Fig. 3c]. For each pixel site i , this value is now defined by the corresponding value in the low-pass filtered image.

The values of $\alpha(l)$, $\beta(l)$, $\gamma(l)$, and σ_i were determined empirically (Table 1 gives the parameter values used). Empirically the parameters were found as follows

Table 1 Parameter values as used in the MRF model for segmentation of metal implants.

	Parameter values			
	α	β	γ	σ
Foreground ($l = 1$)	0	0	150	900
Background ($l = 0$)	0	7	0	300

using an example sinogram: The parameter α was used to tune the initial estimate: to make that at least all metal signal pixels are labeled as foreground. β was used to remove small false positive detections in the background possibly attached to the metal signal. The parameter γ was tuned to strengthen the foreground segmentation where the signal becomes thin and at the borders of the signal. The σ values were estimated from the raw data in the example sinogram.

The values μ_l are determined from the actual raw data: using two-dimensional order-statistic filtering in the ROI, each pixel is replaced by the 90 percentile value of its 50×50 neighborhood and mean foreground values $\mu_l = 1$ are estimated for each pixel site within the ROI [Fig. 3d]. Statistical filtering is used here to create an image containing reasonable estimates of the metal signal in a larger region that covers both the metal signal and the signal's neighborhood. Using an interpolation image, by smoothly interpolating inward from the outer contour of the ROI by solving Laplace's equation,^{17, 18} mean background values $\mu_l = 0$ are retrieved for each pixel site [Fig. 3e].

The model needs an initial estimate of the labeling. This is achieved by applying Eq. (1) with $g(l)$ and $h(C)$ set to zero and by maximizing the probability of pixel labels x_i [Fig. 3f gives an impression of the initial labeling]. Then this labeling result is iteratively adjusted, where $g(l)$ and $h(C)$ are updated before every new iteration step. In each iteration a pixel is marked with the label that gives the highest probability. We applied ten iteration steps since it appeared that the segmentation results become stable within ten iterations [Fig. 3g]. An iteration step takes about 1.6 s (Core2 Duo E8200, 2GB RAM).

Interpolation

Interpolation within the metal region is performed in the original sinogram. Within the mask the difference between the original metal region pixel values and the corresponding interpolated pixel values is determined (as an estimation of the metal signal) and decreased to 10% of its value. Subsequently this scaled difference is added to the interpolated pixel values within the mask. Thus the metal object remains recognizable after application of the metal artifact reduction process [Fig. 3h]. The choice for reduction to 10% of the estimated metal signal is a pragmatic one and appeared to give suitable results.

Three interpolation techniques are applied. In the first approach linear interpolation is applied between the contour pixel sites at each viewing angle,⁵

indicated further as “per view interpolation.” In another approach a function is used that fills in pixels in the segmented implant region by smoothly interpolating from the pixels surrounding the region by solving Laplace’s equation. This will be referred to in this paper as “smooth interpolation.” This approach has been described, for instance, in Refs. ^{17, 18}. Finally, in a third approach, to possibly better preserve the structure of adjacent projections, pairs of pixels are determined on both sides of the implant based on shortest spatial distance (indicated further in this paper as “shortest distance interpolation”). The latter algorithm is derived from the method that was described by Yazdi et al.⁸ Two sets of edge pixels are determined: the set (m) of all edge pixels on one side of the implant region (viewed from the direction of the rows) and the set (n) for all edge pixels on the other side of the region. Then for each pixel p_k belonging to m , the corresponding pixel p_j belonging to n is determined with minimum Euclidean distance $D(p_k, p_j)$, where $D(p_k, p_j)$ is defined according to

$$D(p_k, p_j) = \sqrt{(x_{p_k} - x_{p_j})^2 + (y_{p_k} - y_{p_j})^2}, \quad (2)$$

Here x and y are the coordinates of edge pixels in the raw data. Linear interpolation is performed between the pixel sites accordingly linked. The interpolation result is smoothed using a 5×5 median filter.

Validation of metal artifact suppression

To evaluate the segmentation method in combination with the three interpolation methods quantitatively, CT data of the PMMA phantom with four inserts (Teflon, 2 PVC inserts, titanium) were included in the study. Additionally, the influence on artifact reduction in adding the scaled metal signal to the interpolation values is studied.

Finally, in one experiment, the conventional image-based correction approach, based on work by Kalender et al.,⁵ is applied to the phantom images as a benchmark.

Since it is quite complicated to project the implant into the original geometry for modern multirow spiral scans, we choose to use artificial raw data instead of original raw data. With respect to this a straightforward parallel beam geometry for forward projection and filtered backprojection was used. The forward projection (Radon transform; MATLAB built-in function) comprised 900 projections equally sampled over 360° (which corresponds to the number of views per rotation in the actual raw data).

The image-based artifact suppression was performed as follows: the metal prosthesis is segmented in the original reconstructed slices by thresholding. Both the segmentation results and the original slices are forward projected. The latter gives the artificial raw data and the former serves as a template for the metal region in the artificial raw data. The correction uses linear per view interpolation to replace pixel values in the metal region. The modified artificial raw data are subsequently reconstructed using a Ram–Lak filtered backprojection routine.

To obtain a fair comparison, the conventional image-based approach using

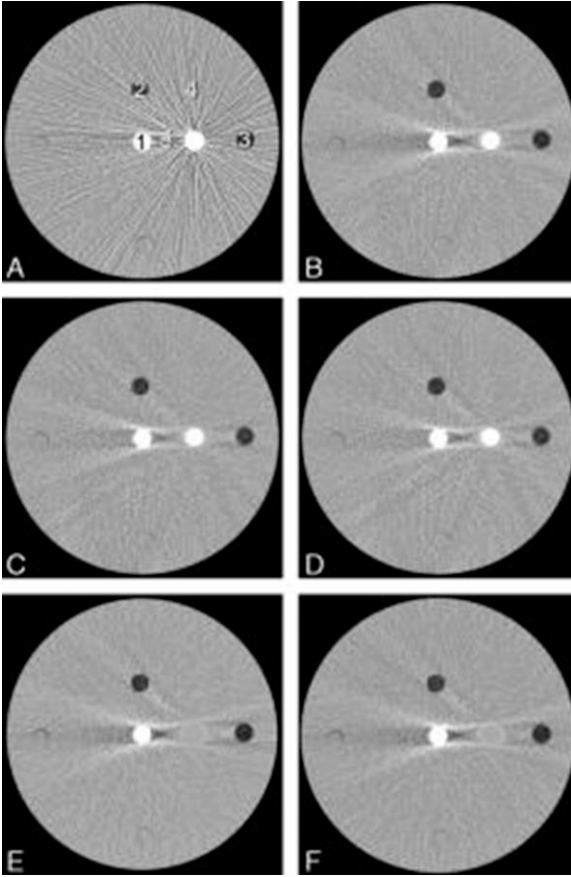


Figure 4 Metal artifact reduction in phantom images. Among other things the effect of different interpolation methods is shown. (a) shows the uncorrected scan. (b) shows the corrected image using the per view interpolation, (c) shows the same detail corresponding to the smooth interpolation, and (d) corresponds to the shortest distance interpolation method. Finally, in (e) a result without adding the scaled projections to the interpolated values is shown when applying the method to artificial raw data instead of original raw data (using smooth interpolation). Additionally, the conventional image-based approach using artificial raw data is shown as a benchmark in (f). Note that the streaking pattern is no longer evident in the images, but the region of reduced density between the objects is still present in the images and more evident in (b) and (f) (per view interpolation).

artificial raw data is compared to our raw data-based method (using smooth interpolation without signal addition) when applied to the same artificial raw data.

The quantitative accuracy of artifact reduction in phantom images was determined by comparing mean HU values and standard deviation (SD) values as a measure of distortion in phantom images with titanium (original and suppressed) and without titanium insert. This was done in 40 consecutive reconstructed slices. Five circular ROIs (each consisting of 300 pixels) per slice

Table 2 Mean CT number and the standard deviation, both measured in HU, for pixels in ROIs (each ROI consisting of 300 pixels) belonging to different inserts in the phantom. Values are based on measurements in 40 consecutive reconstructed slices.

Raw data type	Phantom configuration/Correction method	Region of interest				
		(1) Teflon	(2) PVC	(3) PVC	(4) PMMA	(5) PMMA
Original raw data	Without titanium	902+/-49	-59+/-36	-62+/-30	117+/-36	117+/-36
	With titanium					
	No artifact suppression	889+/-82	-52+/-63	-64+/-85	116+/-72	101+/-98
	Per view interpolation	841+/-47	-49+/-36	-67+/-28	118+/-34	76+/-57
	Shortest distance interpolation	867+/-48	-53+/-37	-52+/-28	118+/-34	99+/-51
	Smooth interpolation	865+/-48	-52+/-36	-54+/-28	119+/-34	90+/-56
Artificial raw data	Smooth interpolation without signal	862+/-48	-52+/-36	-53+/-27	117+/-33	88+/-56
	Without titanium	899+/-30	-62+/-21	-63+/-17	116+/-20	123+/-24
	With titanium					
	Smooth interpolation	835+/-30	-51+/-21	-55+/-17	118+/-20	74+/-50
	Image-based method	832+/-29	-50+/-21	-70+/-17	116+/-20	70+/-52

were used with respect to Teflon, PVC (2x), and PMMA (2x).

CT data of five patients with metal prosthesis were used for clinical evaluation of the proposed raw data-based method (using smooth interpolation). Artifact reduction in clinical scans was evaluated by comparing original patient images with and without artifact suppression on a base of visual inspection. General evaluation of the image quality in the clinical scans concerning all methods was performed qualitatively by a physicist. Clinical evaluation concerning the raw data-based method with smooth interpolation was done by a fellowship-trained radiologist with more than 10 years experience in musculoskeletal radiology. The radiologist quantitatively judged the images by assessing the degree of image quality of original and metal artifact suppressed images on a score of 1–5 (1 = bad image quality, 2 = moderate image quality, 3 = sufficient image quality, 4 = good image quality, and 5 = excellent image quality) with respect to anatomical features. Scores (averaged over patients) for each feature with respect to original and suppressed images were compared on a pairwise basis using Wilcoxon's signed rank test.

Results

The results for the phantom experiment are shown in Fig. 4. In the experiment the three interpolation methods were evaluated quantitatively. The phantom was configured as follows: one titanium rod is located at the right from the center of the phantom between two other inserts. In the phantom's center a Teflon rod is located that simulates bone. At the outer right and above the center two PVC rods are inserted resulting in negative HU values representing fat tissue. The titanium rod simulates a hip or shoulder prosthesis. Figure 4a shows

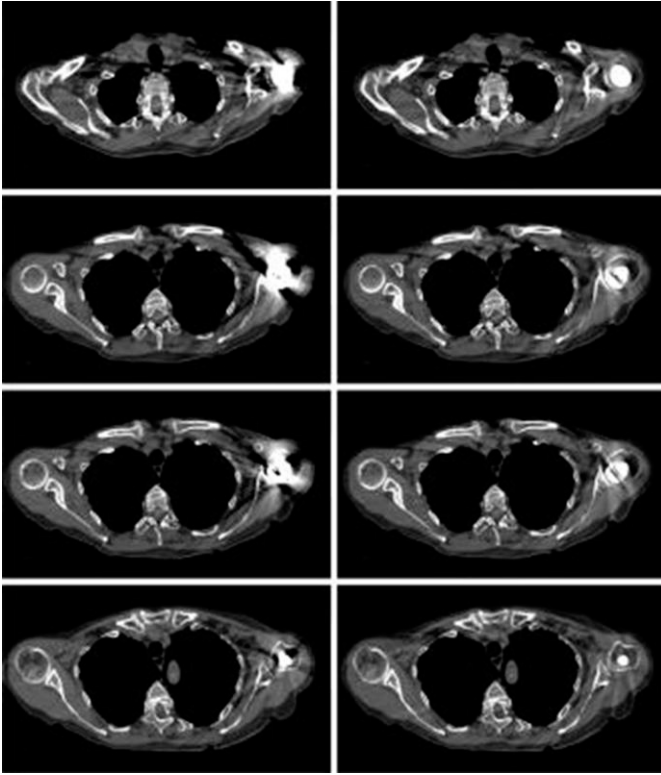


Figure 5 Patient with hip implant. At the left slices of the original scan data are shown. At the right corresponding slices are shown that correspond to corrected raw data (smooth interpolation). The window center and window width were, respectively, 150 and 700 HU for all images.

the uncorrected scan and shows the ROIs used for quantitative analysis. The artifacts introduced by the metal include a streak pattern that radiates from the titanium rod and a low-density (dark) region located between the titanium rod and the Teflon rod in the phantom's center. Figure 4b shows a slice of the corrected image using the per view interpolation, Fig. 4c shows the same slice corresponding to the shortest distance interpolation, and Fig. 4d corresponds to the smooth interpolation method. Finally, in Fig. 4e a result without adding the scaled projections to the interpolated values is shown when applying the method to artificial raw data instead of original raw data (smooth interpolation was used). Additionally, the conventional image-based approach using only artificial raw data is shown as a benchmark in Fig. 4f. For obtaining artificial raw data, in both cases (e and f) the same parallel beam configuration and reconstruction filter were used (as described in Sec. 2D).

Note in all images that the streaking pattern is no longer evident, but the region of reduced density between the objects remains present in the images. Note also that this artifact seems more evident in Figs. 4b,4f, both are based on per view interpolation.

Table 2 gives the results of the quantitative analysis. Measurements are

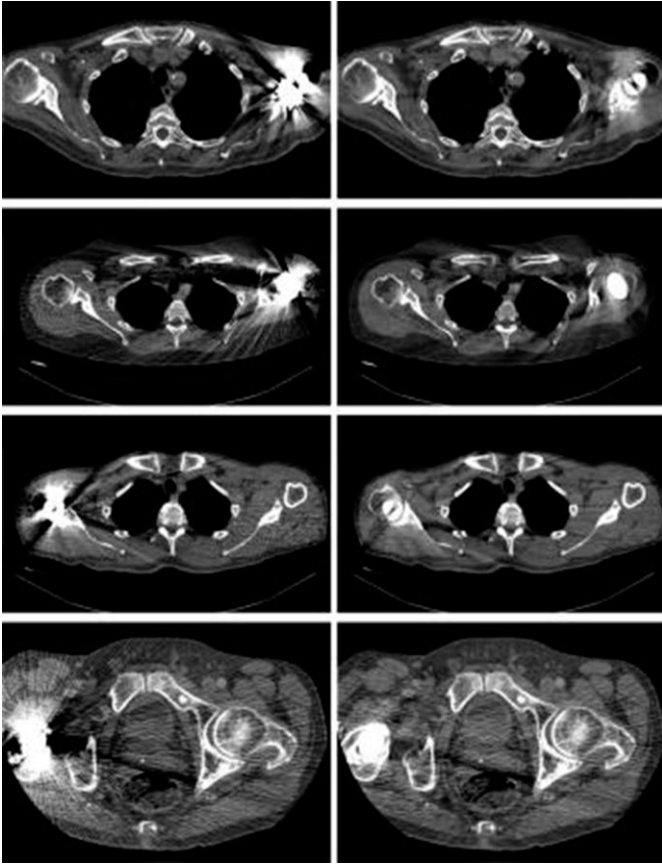


Figure 6 Results of four patients with different implants. At left original slices are shown and at the right slices from corrected raw data are shown. For two patients (images at the top and at the bottom) the window center and window width were, respectively, 60 and 450 HU. For the other two patients (images in the middle) the window center and window width were, respectively, 150 and 700 HU.

performed in five ROIs as shown in Fig. 4a. From quantitative analyses it appeared that all techniques show reduced SD values close to the SD values without titanium insert and thereby improved image quality. The HU values for Teflon in artifact suppressed images are slightly lower compared to images without titanium insert (with smooth interpolation and shortest distance interpolation giving better results than per view interpolation). For PVC (low contrast) the values in corrected images were slightly higher than expected. The per view method gives inconsistent results with respect to the two PVC inserts. The values related to smooth and shortest distance interpolation are more consistent and similar. Furthermore, the artifact is indeed more severe with the per view method according to the mean HU value in ROI 5, where the shortest distance method gives best results. Finally, the smooth interpolation without adding the scaled metal signal appears to give similar results as when adding

10% of the metal signal (as was the case for all other items in the table).

Table 2 also shows measurements concerning comparison of our raw data-based method (using smooth interpolation without signal addition) and the standard image-based approach. For this purpose, both methods are applied to artificial raw data. As a reference for both methods, results for images without titanium insert after consecutive forward and backward projections are given. For all cases the same parallel beam configuration and reconstruction filter were used (as described in Sec. 2D). Twice the number of views in one rotation, as was applied in one experiment, gave similar results. Comparison of the two results for images without titanium insert in Table 2 shows that SD values after consecutive forward and backward projections are strongly reduced due to the low-pass filtering effect of the forward projection and the reconstruction steps. SD values with respect to both the image-based method and the raw data-based method are close to the SD values related to images without titanium insert in case artificial raw data were involved. This indicates that artifacts are successfully suppressed. However, the image-based method gives inconsistent results with respect to the two PVC inserts. The values related to the raw data-based method are more consistent.

Figure 5 shows results of our artifact suppression method (using smooth interpolation) in a patient by comparing four slices. In each case, the left figure represents the uncorrected image and the right figure represents the corrected image. Application of our method strongly reduces metal artifacts. Application of the algorithm shows that the streaking regions as well as the low-density regions are reduced. However, the algorithm does not eliminate all artifacts.

Figure 6 shows the results of the remaining four patients. Again at the left the original slices are shown and at the right the corrected images are depicted (smooth interpolation). In all cases the improvement in image quality is clear. The uncorrected images suffer from strong artifacts, visible as dark and light streaks and by a radiating pattern originating from the implant. The corrected images show elimination of the radiating pattern and of the dark streaks around the implant. Sometimes the method introduces new artifacts, visible as lowered HU values. Similar results were obtained for all three interpolation methods.

Finally, Fig. 7 gives an impression of our raw data-based method [using smooth interpolation; no signal addition; Fig. 7b] in relation to the standard image-based method [Fig. 7c]. In both methods correction is applied to artificial raw data. Visual inspection suggests comparable reduction in artifacts.

For all five patients, the fellowship-trained radiologist judged original and artifact suppressed images for visibility of relevant anatomical details. For artifact suppressed images, the raw data-based method using smooth interpolation was involved. The results are shown in Table 3. In general, the radiologist noticed improved image quality due to a strong reduction in the dark and light streaks and the radiating pattern originating from the implant. In more detail, this appeared to result in substantially improved visibility of axillary lymph nodes (scores 1.8 versus 4.0 for original and processed images,

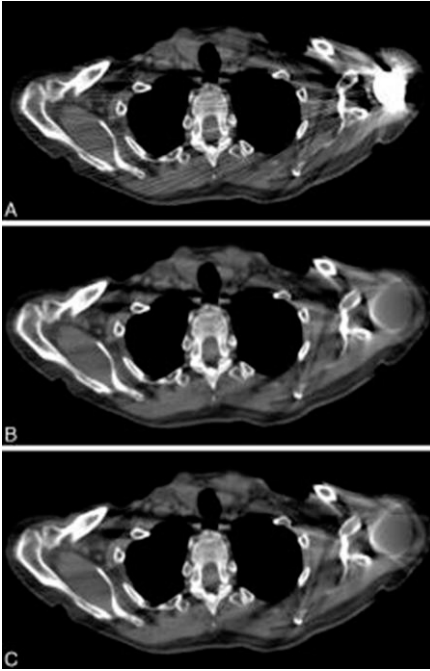


Figure 7 An impression is given of our raw data-based method [using smooth interpolation; (b)] in relation to the standard image-based method (c). Both methods are applied to artificial raw data for this purpose. (a) shows the original slice. The window center and window width were, respectively, 150 and 700 HU for all images.

respectively) and small vascular structures (1.8 versus 3.8) in the metal artifact reduced images of all patients. Also assessment of the prosthesis (2.4 versus 4.0) and the neighboring bone (3.2 and 4.0) was by far more accurate in artifact suppressed images. For shoulder prostheses the visibility of the chest wall (1.8 versus 3.0) improved with artifact suppressed images, whereas for the hip prosthesis patient the visibility of prostate (3.0 versus 4.0) and pelvic wall (2.0 versus 4.0) improved, whereas the visibility of the rectum did not show improvement (4.0 versus 4.0). The overall average scores for original and processed images was, respectively, 2.5 and 3.9 ($p = 0.02$).

Discussion

We have described a method to reduce the magnitude of CT artifacts due to metal prostheses. In both phantom and patient studies, this approach resulted in substantial artifact reduction.

We developed a segmentation method that is capable of segmenting metal structures in original raw CT data. The method is based on the use of Bayesian techniques and application of a Markov random field model. After the metal is segmented, an interpolation method is used in combination with scaling of the

Table 3 For all patients, the fellowship-trained radiologist judged original and artifact suppressed images for visibility and assessment of relevant anatomical details and structures. For artifact suppressed images, the raw data-based method using smooth interpolation was involved. The radiologist quantitatively judged the images (original and processed) on a score from 1–5 (1 = bad image quality, 2 = moderate image quality, 3 = sufficient image quality, 4 = good image quality, and 5 = excellent image quality) for each of the five patients. The average scores for original and processed images were, respectively, 2.5 and 3.9 (p = 0.02).

	Patient 1		Patient 2		Patient 3		Patient 4		Patient 5		Average score	
	Original	Suppressed	Original	Suppressed								
General												
Visibility of												
Lymph nodes	2	4	2	4	1	4	1	4	3	4	1.8	4.0
Small vasc. str.	2	4	2	4	1	4	1	3	3	4	1.8	3.8
Assessment of												
Prosthesis	3	4	3	4	2	4	2	4	2	4	2.4	4.0
Neighboring bone loss	4	4	4	4	3	4	2	4	3	4	3.2	4.0
Shoulder prosthesis												
Assessment of												
Chest wall	2	3	3	3	1	3	1	3			1.8	3.0
Hip prosthesis												
Assessment of												
Prostate									3	4	3.0	4.0
Pelvic wall									2	4	2.0	4.0
Rectum									4	4	4.0	4.0

metal signal, to replace the metal signal by a more appropriate signal intensity. Accordingly, the metal object remains visible in the reconstructed images.

Both in a phantom and in five patients with metal implants, the segmentation method appears to result in improved image quality. In phantom images, the technique showed reduced SD close to the SD for the case where titanium was not inserted. In the patient study a significant ($p = 0.02$) improvement in image quality was found by a fellowship-trained radiologist. Three interpolation methods are investigated. The methods appeared to give similar results but small differences may exist: the smooth interpolation method and the shortest distance method appeared to give more consistent results in the phantom study than the per view interpolation method. Interpolation methods sometimes induce new artifacts. Sinogram information of structures that are overprojected in the metal region is missing or incomplete (due to strong or almost total absorption of the x-ray beams in the patients and insufficient detector sensitivity at very low signals). This aspect hampers successful interpolation and may give rise to new artifacts or may result in a limited suppression of the original artifacts (some artifacts may still be present after the correction procedure). It should be emphasized that the overall result of the method is positive.

More accurate inpainting of the metal region in raw data can potentially be obtained by using the reconstructed images. Applying a dedicated forward projection it should be possible to predict more correct pixel values in the metal region,³ although a problem might be the influence of artifacts that might be forward projected as well. Other methods that may have potential are sinogram decomposition techniques as described in literature.^{3,19}

Our method is different from other papers on this subject. We constructed a segmentation method that performs segmentation and adjustment directly in original raw data. Most methods so far describe segmentation in reconstructed images and use a forward projection to replace projections in raw data. Implementing segmentation and correction directly in original raw CT data or sinograms avoids the need for a complex forward projection with the same geometry as the original raw data (or the disadvantage associated with using a simpler geometry and artificial raw data). Moreover, potentially our method could be faster since the forward projection is omitted. Furthermore, our method can also correct for metal objects that are completely or partly outside the reconstruction field of view, since the disturbing metal parts should always be visible in the original raw data. Initial results suggested comparable improvement in image quality for our raw data-based method and the image-based approach. The comparison was based on correcting artificial raw data obtained from reconstructed images (using a straightforward Radon transform) followed by filtered backprojection of the corrected data. Comparisons using original raw data have to be done in the future to obtain more insight.

The study as described in this paper is performed on one phantom and a limited number of five patients with metal implants. All patients had unilateral prosthesis. It is clear that the presented approaches still have to be evaluated by

experienced radiologists on large numbers of patient studies (including patients with bilateral prostheses) by experienced radiologists. Observer studies need to be performed to study whether the method improves diagnostic accuracy.

In summary, the Markov random field based segmentation method in raw data in combination with a relatively simple interpolation method (i.e., smooth, per view, or shortest distance interpolation) allows for a significant improvement of images that are corrupted by metal artifacts. The design is efficient and the method can correct for metal objects outside the reconstruction field of view.

Reference List

1. Hsieh J, Molthen RC, Dawson CA, Johnson RH. An iterative approach to the beam hardening correction in cone beam CT. *Medical Physics* 2000;27:23-29.
2. Zhao SY, Roberston DD, Wang G, Whiting B, Bae KT. X-ray CT metal artifact reduction using wavelets: Arm application for imaging total hip prostheses. *Ieee Transactions on Medical Imaging* 2000;19:1238-1247.
3. Bal M, Spies L. Metal artifact reduction in CT using tissue-class modeling and adaptive prefiltering. *Med Phys* 2006;33:2852-2859.
4. Glover GH, Pelc NJ. An Algorithm for the Reduction of Metal Clip Artifacts in Ct Reconstructions. *Med Phys* 1981;8:799-807.
5. Kalender WA, Hebel R, Ebersberger J. Reduction of Ct Artifacts Caused by Metallic Implants. *Radiol* 1987;164:576-577.
6. Rinkel J, Dillon WP, Funk T, Gould R, Prevrhal S. Computed Tomographic Metal Artifact Reduction for the Detection and Quantitation of Small Features Near Large Metallic Implants: A Comparison of Published Methods. *Journal of Computer Assisted Tomography* 2008;32:621-629.
7. Mahnken AH, Raupach R, Wildberger JE, Jung B, Heussen N, Flohr TG, Gunther RW, Schaller S. A new algorithm for metal artifact reduction in computed tomography - In vitro and in vivo evaluation after total hip replacement. *Invest Radiol* 2003;38:769-775.
8. Yazdi M, Gingras L, Beaulieu L. An adaptive approach to metal artifact reduction in helical computed tomography for radiation therapy treatment planning: experimental and clinical studies. *Int J Radiat Oncol Biol Phys* 2005;62:1224-1231.
9. Yu HY, Zeng K, Bharkhada DK, Wang G, Madsen MT, Saba O, Policeni B, Howard MA, Smoker WRK. A segmentation-based method for metal artifact reduction. *Academic Radiology* 2007;14:495-504.
10. Zhang Y, Zhang L, Zhu RX, Chambers M, Dong L. Reducing metal artifacts in cone-beam CT by tracking and eliminating metal shadows in raw projection data. *Med Phys* 2006;33:2288.
11. Zhang YB, Zhang LF, Zhu R, Lee AK, Chambers M, Dong L. Reducing metal artifacts in cone-beam CT images by preprocessing projection data. *International Journal of Radiation Oncology Biology Physics* 2007;67:924-932.
12. Kachelriess M. thesis/dissertation. Friedrich-Alexander-Universität Erlangen-Nurnberg; 1998.
13. Ridler TW, Calvard S. Picture Thresholding Using An Iterative Selection Method. *Ieee Transactions on Systems Man and Cybernetics* 1978;8:630-632.
14. Besag J. On the Statistical-Analysis of Dirty Pictures. *Journal of the Royal Statistical Society Series B-Methodological* 1986;48:259-302.
15. Karssemeijer N. A Stochastic-Model for Automated Detection of

- Calcifications in Digital Mammograms. Lecture Notes in Computer Science 1991;511:227-238.
16. Veldkamp WJH, Karssemeijer N. Accurate segmentation and contrast measurement of microcalcifications in mammograms: A phantom study. *Medical Physics* 1998;25:1102-1110.
 17. Elder JH, Goldberg RM. Image editing in the contour domain. *Ieee Transactions on Pattern Analysis and Machine Intelligence* 2001;23:291-296.
 18. Wood JD, Fisher PF. Assessing Interpolation Accuracy in Elevation Models. *Ieee Computer Graphics and Applications* 1993;13:48-56.
 19. Zamyatin AA, Nakanishi S. Extension of the reconstruction field of view and truncation correction using sinogram decomposition. *Medical Physics* 2007;34:1593-1604.

